Nanotechnol. Environ. Eng. (2017) 2:4
https://doi.org/10.1007/s41204-017-0014-y

ORIGINAL PAPER

Fabrication and characterization of a nanocomposite hydrogel for combined photocatalytic degradation of a mixture of malachite green and fast green dye

Gaurav Sharma[1] · Zeid Abdullah ALOthman[2] · Amit Kumar[1] · Shweta Sharma[1] · Senthil Kumar Ponnusamy[3] · Mu. Naushad[2]

Received: 22 December 2016 / Accepted: 15 February 2017 / Published online: 22 March 2017

Abstract In this study, starch/poly(alginic acid-*cl*-acrylamide)/*Fe/Zn* nanocomposite hydrogel (*ST/PL(AA-cl-AAm)/Fe/Zn NCHG*) was synthesized by polymerization/co-precipitation method. This nanocomposite hydrogel was prepared with the notion to remove the mixture of organic pollutants from the water system. Mixture of malachite green and fast green dye was used to check the photocatalytic degradation ability of the prepared nanocomposite hydrogel. *ST/PL(AA-cl-AAm)/Fe/Zn* NCHG was characterized by X-ray diffraction, transmission electron microscopy, scanning electron microscopy and Fourier transform infrared. The degradation of the two dyes followed the pseudo-first-order kinetics. The results showed that by using the prepared nanocomposite hydrogel, 91% of malachite green and 82% of fast green dye, respectively, were degraded within 5 h of their contact.

Keywords Starch · Nanocomposite hydrogel · Alginic acid · Adsorptional photocatalysis

✉ Gaurav Sharma
gaurav8777@gmail.com

✉ Mu. Naushad
mnaushad@ksu.edu.sa

[1] School of Chemistry, Shoolini University, Solan, Himachal Pradesh 173212, India

[2] Advanced Materials Research Chair, Department of Chemistry, College of Science, Bld.#5, King Saud University, Riyadh, Saudi Arabia

[3] Department of Chemical Engineering, SSN College of Engineering, Chennai 603110, India

Introduction

Industrial effluents contribute the most to the addition of various types of dyes into the water system. These dyes not only affect the aquatic life but also disrupt the whole ecosystem. The dyes easily get mixed with the water and reduce the photocatalytic activity of underwater plants, and hence affecting the food chains. In addition, dyes also make the water unfavorable for drinking, irrigation and recreation purposes. Azo dyes are quite toxic and carcinogenic in nature [1]. They easily enter into the body through ingestion and damage the DNA. Workers in textile industries are most prone to respiratory problems caused by the harmful dyes. So, their removal is the major priority. Researchers have tried to remove the dyes from wastewater using different techniques such as osmosis, precipitation, electrokinetic coagulation, microbial degradation, fungal decolorization, electrodialysis, nanofiltration, electrosorption, adsorption and filtration [2–4]. However, adsorption is considered as the best technique for the removal of dyes from the wastewater due to its simple methodology and cost-effectiveness. Different adsorbing materials such as hydrogels, activated carbon and clay minerals have been used for the removal of dyes.

Hydrogels are the three-dimensional network materials having high adsorbing ability. Their water adsorbing ability is due to the hydrophilic groups present in their structure. The organic pollutants get adsorb into hydrogels as the ionic groups of organic pollutants form physical or chemical interaction with hydrophilic groups of hydrogels [5–10]. The addition of reinforcing agents and using crosslinkers during their synthesis helps in increasing the mechanical strength of the hydrogels. Changing the pH, temperature, agitation time, etc. during synthesis of hydrogels helps in tailoring their properties. Their

application area includes drug delivery in a controlled manner, tissue engineering, micro-irrigation, etc. [11–17].

Nanocomposite hydrogels contain both organic and inorganic counterparts. They bridge the gap between organic and inorganic counterparts and also overcome the nonuniformity at the structural level [18–21]. A major breakthrough occurred when Haraguchi et al. prepared the first ever nanocomposite hydrogel using free radical polymerization. These days, number of materials has been used such as carbon nanotubes, graphene oxide, carbon dots, metal oxides and ceramics, etc. so as to make novel nanocomposite hydrogels having improved mechanical properties [22–25].

The use of nanocomposite hydrogel materials as a photocatalyst is one of the recent inventions which help in the removal of organic pollutants from the wastewater. The photocatalytic ability of these composites helps in monitoring and improving the ecosystem [26–29]. They actually remove the toxic organic pollutants to the maximum extent under different conditions. These are the most preferred materials due to their low cost and almost nil production of harmful by-products [30, 31].

In the present paper, a novel starch/poly(alginic acid-cl-acrylamide)/Fe/Zn nanocomposite hydrogel (ST/PL(AA-cl-AAm)/Fe/Zn NCHG) has been synthesized and the ability of this nanohydrogel composite for the adsorptional photocatalytic degradation of mixture of malachite green and fast green dye has been reported.

Experimental

Chemicals and reagents used

Ferric nitrate, zinc nitrate, starch, ammonium per sulfate and sodium borohydride were obtained from CDH Pvt. Ltd, India. Alginic acid and acryl amide were purchased from Loba Chemie Pvt. Ltd, India. *N*,*N*′-methylene bis-acryl amide was obtained from S-D Fine Chem. Limited.

Apparatus

Electronic balance (Kerro BLC 3002), centrifuge machine (Instruments, chemical private limited), oven (NSW India) and UV–visible spectrometer (INCO Instrument and Chemical Private Limited). X-ray diffractometer (Philips 1830 diffractometer), transmission electron microscope (Techni G2 20 S-Twin), Fourier transform infrared (FTIR) spectrophotometer (Nicolet 5700 FTIR Spectrophotometer) and scanning electron microscope (JSM 6100) were used for the characterization of the synthesized nanocomposite hydrogel.

Preparation of reagents

2 M solution of acryl amide, 1 M solution of alginic acid, 1% starch solution, 0.1 M ferric nitrate solution, 0.1 M zinc nitrate solution, 0.1 M sodium borohydride solution, 5% ammonium per sulfate (weight of acryl amide, alginic acid and starch) as an initiator and 3% *N*,*N*′-methylene bis-acryl amide (weight of acryl amide, alginic acid and starch) as a crosslinker were used and prepared in double-distilled water.

Synthesis of *ST/PL(AA-cl-AAm)/Fe/Zn* NCHG

The *ST/PL(AA-cl-AAm)/Fe/Zn* NCHG was synthesized by polymerization/co-precipitation method. 1 M alginic acid solution and 1% starch solution were added to the 2 M solution of acryl amide dropwise with constant stirring. Then, 5% ammonium persulfate as an initiator and 3% *N*,*N*′-methylene bis-acrylamide as a crosslinker were added with constant stirring. The resultant mixture was stirred for 5 h at 65 °C over the magnetic stirrer with hot plate. The obtained precipitates of *ST/PL(AA-cl-AAm)* NHG were filtered, washed and dried in hot air oven at 50 °C. The precipitates were then added to the mixture of 0.1 M ferric nitrate and 0.1 M zinc nitrate solution and stirred for 4 h. Finally, precipitates were filtered and added to the 0.1 M solution of sodium borohydride, and the solution was made to remain as such for 3 h. The obtained precipitates were filtered, washed and dried in hot air oven at 50 °C. The % yield of the reaction was calculated by using following formula [32]:

$$\%\,\text{yield} = \frac{W_{\text{R}} - W_{\text{P}}}{W_{\text{R}}} \times 100 \quad (1)$$

where W_{R} is the weight of reactants and W_{P} is the weight of product.

Characterization

Fourier transform infrared (FTIR) spectroscopy

The Fourier transform infrared spectrum of *ST/PL(AA-cl-AAm)/Fe/Zn* NCHG was recorded using Nicolet 5700 FTIR spectrophotometer. Spectrum was documented in the range of 400–4000 cm^{-1}. The nanocomposite hydrogels were methodically mixed with KBr and were then powdered. A pressure of about 80,000 psi was applied to make a transparent disk and it was then completely characterized to find the type of functional groups present [33].

X-ray diffraction (XRD)

X-ray diffraction data were recorded using X-ray diffractometer (Philips 1830 diffractometer). It helped in

examining the nature of synthesized *ST/PL(AA-cl-AAm)/Fe/Zn* NCHG.

Scanning electron microscopy (SEM)

Scanning electron microscopy (SEM) is the most widely used instrument to characterize the physical properties such as morphology, shape and size distribution of materials at the micro- and nanoscale. SEM helps in the identification and also for the morphological characterization of nanocomposites. SEM uses high-energy electron beam. This electron beam interacts with the sample and helps to appraise the surface and morphological identification of the *ST/PL(AA-cl-AAm)/Fe/Zn* NCHG [34]. The surface and morphological studies of *ST/PL(AA-cl-AAm)/Fe/Zn* NCHG were carried out using scanning electron microscope JSM 6100.

Transmission electron microscopy (TEM)

Transmission electron microscopy (TEM) images of the *ST/PL(AA-cl-AAm)/Fe/Zn* NCHG was recorded using Techni G2 20 S-Twin. It is basically an electron-based technique that uses transmitted electrons for the elucidation of the structure, shape and size of the sample. In this technique, ultrasonicated nanocomposite hydrogel was loaded on gold-coated grid and a transmitted electron beam was detected on the other side which helped in the structural exploration.

Adsorptional photocatalysis

The adsorptional photocatalytic activity of *ST/PL(AA-cl-AAm)/Fe/Zn* NCHG was explored for the degradation of mixture of malachite green and fast green dye in the presence of solar light. A double-walled Pyrex glass chamber was jacketed with thermostatic water circulation to carry out the photocatalytic experiments. A constant temperature of 25 °C ± 1 was maintained throughout the experiment. 100 mg of the *ST/PL(AA-cl-AAm)/Fe/Zn* NCHG was added into 2×10^{-6} M solution of malachite and fast green dye to form slurry [35, 36]. The slurry was subjected firstly to adsorption for 1 h kept in dark to attain the adsorption–desorption equilibrium, and after that, it was directly exposed to sunlight for photocatalysis. Nearly around 3 mL of the dye solution was withdrawn at various time intervals and centrifuged to confiscate particles of the *ST/PL(AA-cl-AAm)/Fe/Zn* NCHG. The absorbance was recorded in the range of 300–750 nm, and the kinetics of the adsorptional photocatalytic degradation of mixture of dyes was investigated at 620 nm for MG and 625 nm for FG. The percent degradation of dye was calculated by using following formula [37]:

$$\% \text{ degradation} = \frac{C_0 - C_t}{C_0} \times 100 \quad (2)$$

where C_0 and C_t are the concentrations of dye at equilibrium and at time t.

Results and discussion

Synthesis of *ST/PL(AA-cl-AAm)/Fe/Zn* NCHG

The *ST/PL(AA-cl-AAm)/Fe/Zn* NCHG was synthesized using polymerization/co-precipitation method. *ST/PL(AA-cl-AAm)* NHG was prepared by the addition of 1 M alginic acid, 1% starch solution and 2 M acrylamide solution in the presence of crosslinker *N*,*N*′-methylene bis-acrylamide and initiator ammonium per sulfate. The obtained precipitates of *ST/PL(AA-cl-AAm)* NHG were then made to react with ferric nitrate and zinc nitrate, which resulted in the desired nanocomposite hydrogel, ST/PL(AA-cl-AAm)/Fe/Zn NCHG. The reaction yield of *ST/PL(AA-cl-AAm)/Fe/Zn* NCHG was found to be 88%.

Characterization

Fourier transform infrared spectra of *ST/PL(AA-cl-AAm)/Fe/Zn* NCHG are shown in Fig. 1. The peaks between 1078 and 1022 cm^{-1} indicated the characteristic peaks of the crystalline and amorphous structure of starch, respectively [34]. The absorption peaks at 926 and 881 cm^{-1} were assigned to the cyclic ether groups [38]. The projecting peaks at 3333.915 and 1727.489 cm^{-1} were due to –OH and C=O stretching functionalities. The peaks at 459 and 559 cm^{-1} were due to the Fe–O and Zn–O stretching [39, 40]. The XRD pattern of the *ST/PL(AA-cl-AAm)/Fe/Zn* NCHG is shown in Fig. 2. The diffractrogram of *ST/PL(AA-cl-AAm)/Fe/Zn* NCHG showed broad peaks at $2\theta = 18.1°$, 30.155°, 34.54°, 43.1°, 56.6° and 70.4° for iron and zinc [41–45]. Three diffraction peaks centered at

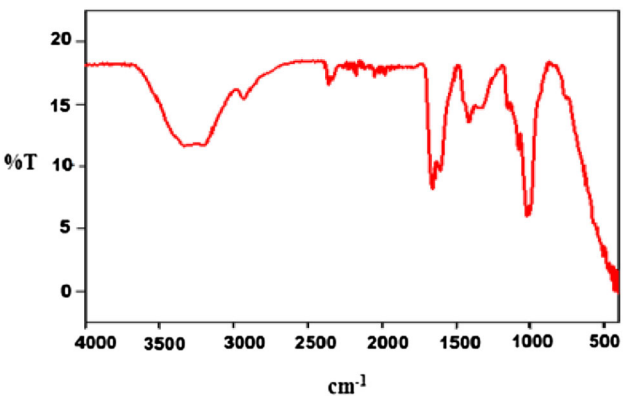

Fig. 1 FTIR spectra of *ST/PL(AA-cl-AAm)/Fe/Zn* NCHG

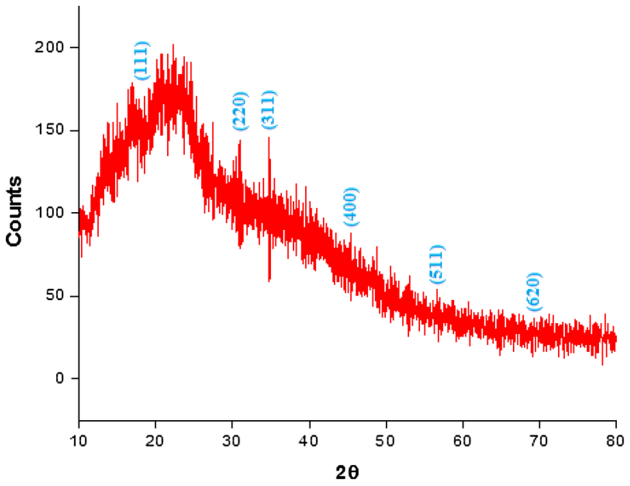

Fig. 2 XRD of *ST/PL(AA-cl-AAm)/Fe/Zn* NCHG

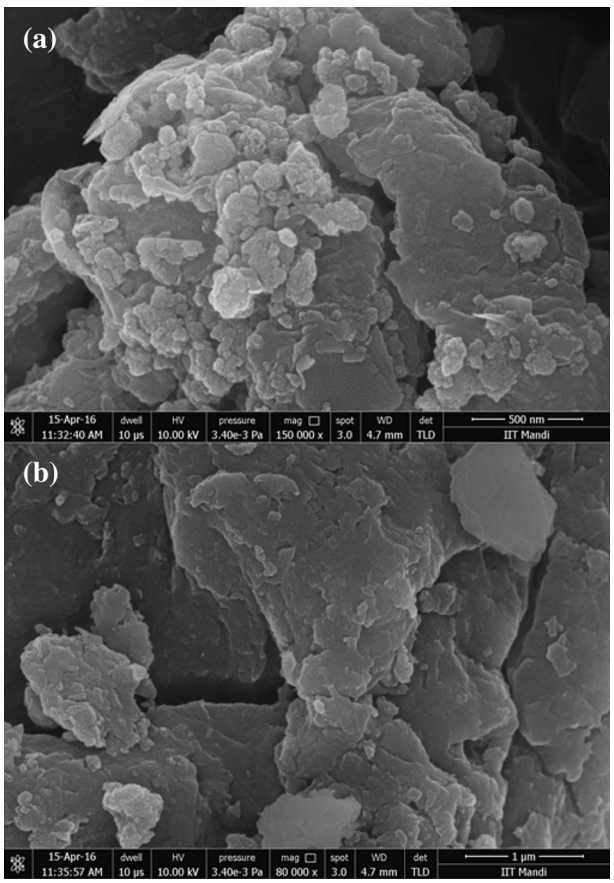

Fig. 3 **a**, **b** SEM images of *ST/PL(AA-cl-AAm)/Fe/Zn* NCHG

$2\theta = 30.155°$, 34.54° and 43.1° were observed for iron, which can be assigned to (220), (311) and (400) diffraction planes, respectively. Three diffraction peaks centered at 18.1°, 56.6° and 70.4° are observed for zinc, which can be assigned to (111), (511) and (620) planes, respectively. The

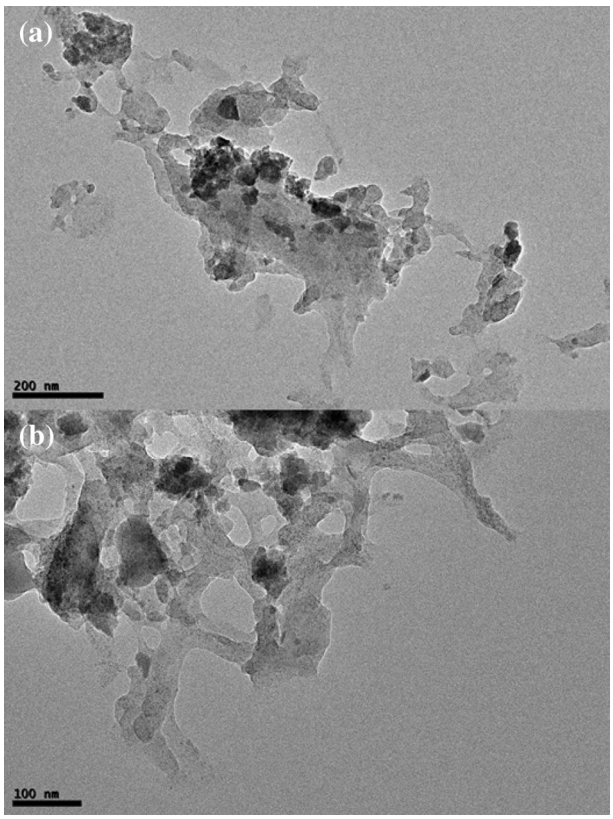

Fig. 4 **a**, **b** TEM images of *ST/PL(AA-cl-AAm)/Fe/Zn* NCHG

XRD results confirm the semicrystalline nature of *ST/PL(AA-cl-AAm)/Fe/Zn* NCHG. Figure 3a, b shows the SEM images of *ST/PL(AA-cl-AAm)/Fe/Zn* NCHG at different magnifications. It indicates the irregular and rough nature of the synthesized *ST/PL(AA-cl-AAm)/Fe/Zn* NCHG. TEM images of *ST/PL(AA-cl-AAm)/Fe/Zn* NCHG are shown in Fig. 4a, b at different magnifications. TEM images confirmed the binding between Fe/Zn and *ST/PL(AA-cl-AAm)* NHG. The average size ranges from 40 to 90 nm for *ST/PL(AA-cl-AAm)/Fe/Zn* NCHG.

Applications

Photocatalytic activity

The photocatalytic degradation of mixture of malachite green and fast green dye by *ST/PL(AA-cl-AAm)/Fe/Zn* NCHG is shown in Fig. 5a–c. Figure 5a decapitates the changes in absorbance spectrum of malachite green and fast green dye with degradation time. The process of photocatalytic activity occurs in two steps: adsorption and adsorptional photocatalysis [46]. It was observed that maximum 20% of mixture of malachite green and fast green dye get adsorbed after 1 h of contact time and 71 and 62% of malachite green and fast green dye undergoes

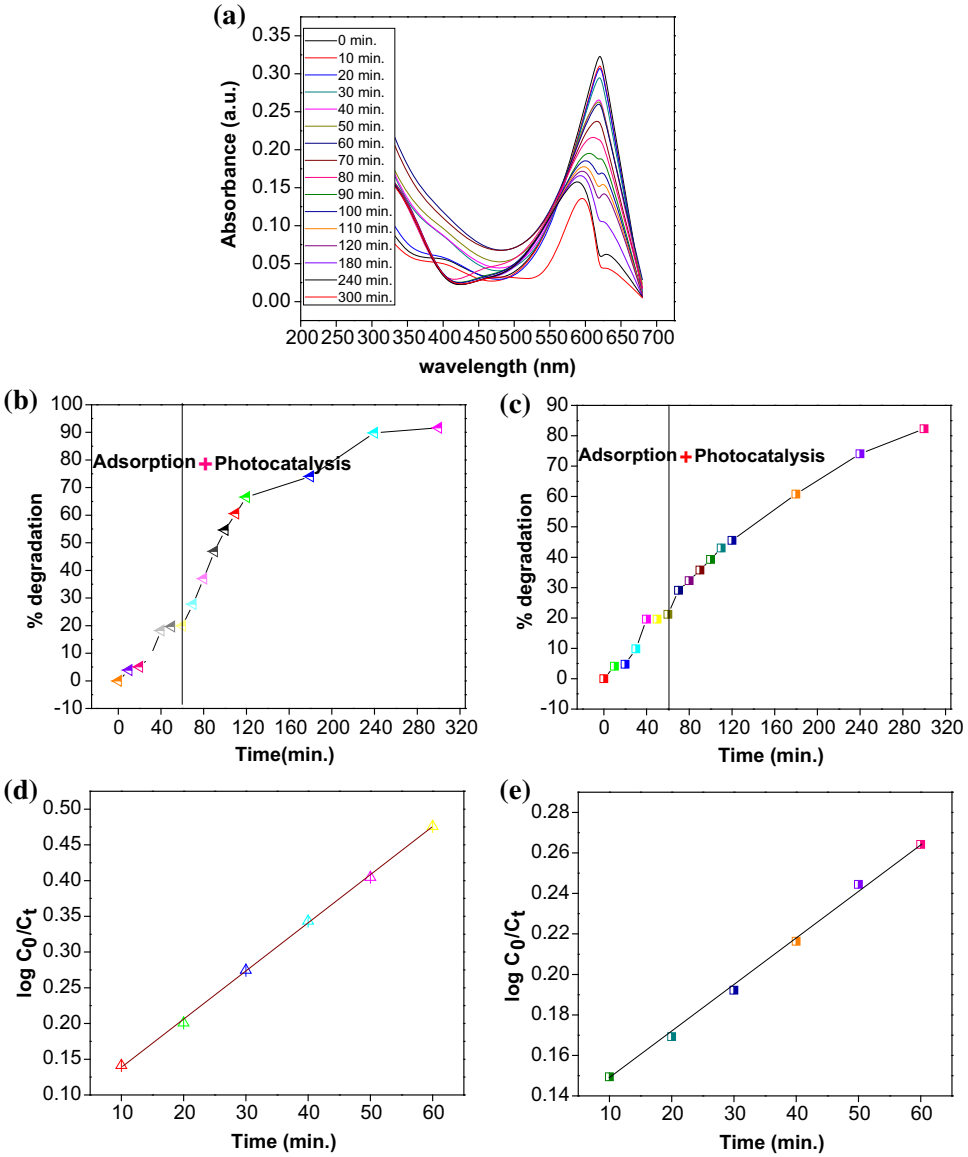

Fig. 5 Degradation and kinetics plots for mixture of malachite green and fast green dye under coupled process in the presence of *ST/PL(AA-cl-AAm)/Fe/Zn* NCHG. **a** Spectrum of malachite green and fast green dye, **b** percent removal of malachite dye, **c** percent removal of fast green dye, **d** pseudo-first-order kinetics for degradation of malachite dye and **e** pseudo-first-order kinetics for degradation of fast green dye

photocatalysis in 4 h of photoperiod, respectively. About 91% of malachite green and 82% of the fast green dye were degraded within 5 h of combined adsorptional photocatalysis process as shown in Fig. 5b, c. The rate of photocatalytic degradation of different dyes has been reported to follow pseudo-first-order kinetic model [47–51]:

$$r = \frac{\mathrm{d}c}{\mathrm{d}t} = K_{\mathrm{app}}t \tag{3}$$

On integrating the above equation, we get

$$\ln \frac{C_0}{C_t} = K_{\mathrm{app}}t \tag{4}$$

where K_{app} is the apparent rate constant, C_0 is the concentration of dye before illumination and C_t is the concentration of dye at time t.

The plot of In C_0/C_t versus irradiation time showed a linear correlation with good precision as shown in Fig. 5d, e. Thus, it reveals that the degradation of the two dyes follows pseudo-first-order kinetics [52]. Rate constant of 0.0102 and 0.0019 min^{-1} was observed for malachite green and fast green dye, respectively. The dye degradation under the combined adsorptional photocatalysis process can be schematically represented as:

$$ST/PL(AA{-}cl{-}AAm)/Fe/Zn + \text{Dyes(D)} \rightarrow ST/PL(AA{-}cl{-}AAm)/Fe/Zn - \text{D}_{ads}$$

$$ST/PL(AA{-}cl{-}AAm)/Fe/Zn - \text{D}_{ads} + hv \rightarrow ST/PL(AA{-}cl{-}AAm)/Fe/Zn - \text{D}^{*}_{ads}$$

$$ST/PL(AA{-}cl{-}AAm)/Fe/Zn - \text{D}^{*}_{ads} \rightarrow ST/PL(AA{-}cl{-}AAm)/Fe/Zn - \text{D}^{+}_{ads} + \text{e}^{-}_{CB}$$

$$\text{e}^{-}_{CB} + \text{O}_2 \rightarrow {}^{\cdot}\text{O}^{-}_{2}$$

$${}^{\cdot}\text{O}^{-}_{2} + \text{D}^{+}_{ads} \rightarrow \text{degradation product}$$

Conclusion

The synthesis of the starch-based nanocomposite hydrogel (*ST/PL(AA-cl-AAm)/Fe/Zn* NCHG) has been carried out by simple polymerization/co-precipitation method. It has been used for the photocatalytic degradation of the mixture of two dyes (malachite green and fast green dye), and the results showed that different degradation percentage was observed. The results showed that by using the prepared nanocomposite hydrogel, 91 and 82% of malachite green and fast green dye, respectively, were degraded within 5 h of their contact. The degradation of both the dyes follows pseudo-first-order kinetics. In future, more emphasis will be laid on modifying the prepared nanocomposite hydrogel so as to make it compatible for numerous dyes.

Acknowledgements We would like to thank Shoolini University, Solan for providing the infrastructure and laboratory facilities to carry out the research work.

References

1. Gupta VK, Pathania D, Priya B, Singha AS, Sharma G (2014) Microwave induced synthesis of graft copolymer of binary vinyl monomer mixtures onto delignified Grewia optiva fiber: application in dye removal. Fronti Chem 2:1–9
2. Kudo A, Miseki Y (2009) Heterogeneous photocatalyst materials for water splitting. Chem Soc Rev 38:253–278
3. Alqadami AA, Naushad M, Abdalla MA, Khan MR, ALOthman ZA (2016) Adsorptive removal of toxic dye using Fe_3O_4–TSC nanocomposite: equilibrium, kinetic, and thermodynamic studies. J Chem Eng Data 61:3806–3813
4. Sharma G, Naushad M, Al-Muhtaseb AH, Kumar A, Khan MR, Kalia S, Sharma S, Bala M, Sharma A (2017) Fabrication and characterization of chitosan-crosslinked-poly (alginic acid) nanohydrogel for adsorptive removal of Cr(VI) metal ion from aqueous medium. Int J Biol Macromol 95:484–493
5. Gong JP (2010) Why are double network hydrogels so tough? Soft Matter 6:2583–2590
6. Pandian AMK, Karthikeyan C, Rajasimman M (2017) Isotherm and kinetic studies on adsorption of malachite green using chemically synthesized silver nanoparticles. Nanotechnol Environ Eng 2:2
7. Hu J, Hiwatashi K, Kurokawa T, Liang SM, Wu ZL, Gong JP (2011) Microgel-reinforced hydrogel films with high mechanical strength and their visible mesoscale fracture structure. Macromolecules 44:7775–7781
8. Yuan N, Xua L, Zhang L, Ye H, Zhao J, Liu Z, Rong J (2016) Superior hybrid hydrogels of polyacrylamide enhanced by bacterial cellulose nanofiber clusters. Mater Sci Eng C 67:221–230
9. Luo ZL, Yue YY, Zhang YF, Yuan X, Gong JP, Wang LL, He B, Liu Z, Sun YL, Liu J, Hu MF, Zheng J (2013) Designer D-form self-assembling peptide nanofiber scaffolds for 3-dimensional cell cultures. Biomaterials 34:4902–4913
10. El-Mohdy HLA, Safrany A (2008) Preparation of fast response superabsorbent hydrogels by radiation polymerization and crosslinking of *N*-isopropylacrylamide in solution. Radiat Phys Chem 77:273–279
11. Jiang FZ, Wang XZ, He CC, Saricilar S, Wang HL (2015) Mechanical properties of tough hydrogels synthesized with a facile simultaneous radiation polymerization and cross-linking method. Radiat Phys Chem 106:7–15
12. Zhao J, Jiao KX, Yang J, He CC, Wang HL (2013) Mechanically strong and thermosensitive macromolecular microsphere composite poly(*N*-isopropylacrylamide) hydrogels. Polymer 54:1596–1602
13. Yasuda K, Gong JP, Katsuyama Y, Nakayama A, Tanabe Y, Kondo E, Ueno M, Osada Y (2005) Biomechanical properties of high-toughness double network hydrogels. Biomaterials 26:4468–4475
14. Schexnailder PJ, Gaharwar AK, Bartlett RL, Seal BL, Schmidt G (2010) Tuning cell adhesion by incorporation of charged silicate nanoparticles as cross-linkers to polyethylene oxide. Macromol Biosci 10:1416–1423
15. Johnson JA, Turro NJ, Koberstein JT, Mark JE (2010) Some hydrogels having novel molecular structures. Prog Polym Sci 35:332–337
16. Haraguchi K, Li H, Ren H, Zhu M (2010) Modification of Nanocomposite gels by irreversible rearrangement of polymer/clay network structure through drying. Macromolecules 43:9848–9853
17. Haraguchi K (2007) Nanocomposite hydrogels. Curr Opin Solid State Mater Sci 11:47–54
18. Mohapatra DP, Kirpalani DM (2017) Process effluents and mine tailings: sources, effects and management and role of nanotechnology. Nanotechnol Environ Eng 2:1
19. Ahmed MA, Abou-Gamra ZM (2016) Mesoporous MgO nanoparticles as a potential sorbent for removal of fast orange and bromophenol blue dyes. Nanotechnol Environ Eng 1:10
20. Haraguchi K, Takehisa T, Fan S (2002) Effects of clay content on the properties of nanocomposite hydrogels composed of poly(*N*-isopropylacrylamide) and clay. Macromolecules 35:10162–10171
21. Sofos M, Goldberger J, Stone DA, Allen JE, Ma Q, Herman DJ, Tsai WW, Lauhon LJ, Stupp SI (2009) A synergistic assembly of nanoscale lamellar photoconductor hybrids. Nat Mater 8:68–75
22. Liu ZQ, Yang ZP, Luo YL (2012) Swelling, pH sensitivity, and mechanical properties of poly(acrylamide-co-sodium methacrylate) nanocomposite hydrogels impregnated with carboxyl-functionalized carbon nanotubes. Polym Compos 33:665–674
23. Zhong EN, Wang T, Nian CX, Sun WX, Liu XX, Tong Z (2013) Robust and thermo-response graphene–PNIPAm hybrid hydrogels reinforced by hectorite clay. Carbon 62:117–126
24. Huang YW, Zeng M, Ren J, Wang J, Fan LR, Xu QY (2012) Preparation and swelling properties of graphene oxide/poly(-acrylic acid-co-acrylamide) super-absorbent hydrogel nanocomposites. Colloids Surf A 401:97–106
25. Ye L, Tang YJ, Qiu D (2014) Enhance the mechanical performance of polyacrylamide hydrogel by aluminium-modified colloidal silica. Colloids Surf A 447:103–110

26. Sharma G, Naushad M, Kumar A, Devi S, Khan MR (2015) Lanthanum/cadmium/polyaniline bimetallic nanocomposite for the photodegradation of organic pollutant. Iran Polym J 24:1003–1013
27. Zhang C, Tian W, Xu Z, Wang X, Liu J, Li SL, Tang DM, Liu D, Liao M, Golberg DBY (2014) Photosensing performance of branched CdS/ZnO heterostructures as revealed by in situ TEM and photodetector tests. Nanoscale 6:8084–8090
28. Tian W, Zhang C, Zhai T, Li SL, Wang X, Liu J, Jie X, Liu D, Liao M, Koide Y, Golberg D, Bando Y (2014) Flexible ultraviolet photodetectors with broad photoresponse based on branched ZnS–ZnO heterostructure nanofilms. Adv Mater 26:3088–3093
29. Sharma G, Gupta VK, Agarwal S, Kumar A, Thakur S (2016) Fabrication and characterization of Fe@MoPO nanoparticles: ion exchangebehavior and photocatalytic activity against malachite green. J Mol Liq 219:1137–1143
30. Cheng C, Liu B, Yang H, Zhou W, Sun L, Chen R, Yu SF, Zhang J, Gong H, Sun H, Fan HJ (2009) Hierarchical assembly of ZnO nanostructures on SnO_2 backbone nanowires: low-temperature hydrothermal preparation and optical properties. ACS Nano 3:3069–3076
31. Hou H, Wang L, Gao F, Wei G, Tang B, Yang W, Wu T (2014) General strategy for fabricating thoroughly mesoporous nanofibers. J Am Chem Soc 136:16716–16719
32. Pathania D, Gupta D, Al-Muhtase A, Sharma G, Kumar A, Naushad M, Ahamad T, Alshehri SM (2016) Photocatalytic degradation of highly toxic dyes using chitosan-g-poly(acrylamide)/ZnS in presence of solar irradiation. J Photochem Photobiol A Chem 329:61–68
33. Naushad M, Ahamad T, Sharma G, Al-Muhtase AZ, Albadarin AB, Alam MM, ALOthman ZA, Alshehri SM, Ghfar AA (2016) Synthesis and characterization of a new starch/SnO_2 nanocomposite for efficient adsorption of toxic Hg_2+ metal ion. Chem Eng J300:306–316
34. Yu QM, Tanaka Y, Furukawa H, Kurokawa T, Gong JP (2009) Direct observation of damage zone around crack tips in double-network gels. Macromolecules 42:3852
35. Liu S, Sun H, Liu S, Wang S (2013) Graphene facilitated visible light photodegradation of methylene blue over titanium dioxide photocatalysts. Chem Eng J 214:298–303
36. Her CY, Yeh YB, Huang LS (2014) Vapor solid growth of p-Te/n-SnO_2 hierarchical heterostructures and their enhanced room-temperature gas sensing properties. ACS Appl Mater Interfaces 6:9150–9159
37. Li SZ, Luo JW, Zhang LM, Feng YJ, Zou GZ (2013) Photoelectrochemical cells for solar hydrogen production: current state of promising photoelectrodes, methods to improve their properties and outlook. Energy Environ Sci 6:347–370
38. Hu J, Kurokawa T, Hiwatashi K, Nakajima T, Wu ZL, Liang SM, Gong JP (2012) Structure optimization and mechanical model for microgel-reinforced hydrogels with high strength and toughness. Macromolecules 45:5218–5228
39. Sharma G, Pathania D, Naushad M (2014) Fabrication, characterization and antimicrobial activity of polyaniline Th(IV) tungstomolybdophosphate nanocomposite material: efficient removal of toxic metal ions from water. Chem Eng J 251:413–421
40. Miller FA, Wilkins CH (1952) Infrared spectra and characteristic frequencies of inorganic ions. Anal Chem 24:1253–1294
41. Pathania D, Gupta D, Kothiyal NC, Sharma G, Eldesoky GE, Naushad M (2016) Preparation of a novel chitosan-g-poly(acrylamide)/Zn nanocomposite hydrogel and its applications for controlled drug delivery of ofloxacin. Int J Bio Macromol 84:340–348
42. Sharma G, Kumar A, Naushad M, Pathania D, Sillanpa M (2016) Polyacrylamide@ Zr(IV) vanadophosphate nanocomposite: ion exchange properties, antibacterial activity, and photocatalytic behavior. J Ind Eng Chem 33:201–208
43. Kumar A, Sharma G, Naushad M, Singh P, Kalia S (2014) Polyacrylamide/$Ni_{0.02}Zn_{0.98}O$ nanocomposite with high solar light photocatalytic activity and efficient adsorption capacity for toxic dye removal. Ind Eng Chem Res 53:15549–15560
44. Cornell RM, Schwertmann U (2003) The iron oxides: structure, properties, reactions, occurrences and uses. Wiley, London
45. Wang Y, Zhao H, Zhaoa G (2015) Iron–copper bimetallic nanoparticles embedded within ordered mesoporous carbon as effective and stable heterogeneous Fenton catalyst for the degradation of organic contaminants. Appl Catal B 164:396–406
46. Pathania D, Katwal R, Sharma G, Naushad M, Rizwan M (2016) Novel guar gum/Al_2O_3 nanocomposite as an effective photocatalyst for the degradation of malachite green dye. Int J Biol Macromol 87:366–374
47. Savic JZ, Vasic VM (2006) Thermodynamics and kinetics of 1,8-dihydroxy-2-(imidazol-5-ylazo)-naphthalene-3,6-disulphonic acid immobilization on Dowex resin. Colloids Surf A Physico Eng Aspects 278:197–203
48. Zhao G, Li J, Xiangke W (2011) Kinetic and thermodynamic study of 1-naphthol adsorption from aqueous solution to sulfonated graphene nanosheets. Chem Eng J 173:185–190
49. Li N, Liu SQ, Zheng T, Wang P, Jiang PJ (2010) Adsorption isotherm, kinetic and mechanism studies of some substituted phenols on activated carbon fibers. Chem Eng J 157:348–356
50. Rupa AV, Manikandan D, Divakar D, Sivakumar T (2007) Effect of deposition of Ag on TiO_2 nanoparticles on the photodegradation of reactive yellow-17. J Hazard Mater 147:906–913
51. Xu J, Ao Y, Fu D, Yuan C (2008) Low-temperature preparation of F-doped TiO_2 film and its photocatalytic activity under solar light. Appl Surf Sci 254:3033–3038
52. Naushad M, Vasudevan S, Sharma G, Kumar A, ALOthman ZA (2016) Adsorption kinetics, isotherms and thermodynamic studies for Hg^{2+} adsorption from aqueous medium using alizarin red-S loaded amberlite IRA-400 resin. Desalin Water Treat 57:18551–18559